Spin-orbit coupling effects on predicting defect properties with hybrid functionals: A case study in CdTe

Jie Pan,* Wyatt K. Metzger, and Stephan Lany†
Materials Science Center, National Renewable Energy Laboratory, Golden, Colorado 80401, USA

(Received 11 May 2018; published 22 August 2018)

Defect formation energies and transition levels are critical in determining doping behavior and recombination in semiconductor applications. Hybrid functionals are often used to overcome the band gap and delocalization errors of standard density-functional theory, and it is tempting to presume that the defect properties are correctly predicted once the hybrid functional mixing parameter reproduces the experimental band gap. However, pronounced spin-orbit coupling (SOC) effects can have an additional important role, which is clearly shown in this work by analyzing SOC effects originating from the Te-p orbitals in CdTe. In this work, we therefore use a hybrid functional that reproduces the experimental band gap when SOC is included, requiring a larger mixing parameter $\alpha = 0.33$ compared to the conventional choice of $\alpha = 0.25$. This hybrid functional was then used to predict defect properties, e.g., formation energy, transition level, and defect equilibrium. For defect states that do not directly involve the Te-p orbitals, such as the Cd interstitial (Cd_i), we find that the effect of SOC on the defect levels can be captured by simply considering the SOC-induced band-edge shift. This is not the case for the A center ($Cl_{Te} - V_{Cd}$ defect pair), where the localized acceptor state formed by Te-p orbitals is more directly affected by the SOC. For this defect, a mixing parameter as large as $\alpha = 0.40$ is required to reproduce the experimental acceptor level. Regarding the implications for photovoltaics, we suggest that the Cd_i, which is the dominant compensating donor, could play an important role as a recombination center. While Cd_i is usually thought of as a benign shallow donor, our predicted defect levels in the fully band-gap-corrected calculations are deep enough to raise a concern, and we propose a recombination mechanism for electron capture by Cd_i.

DOI: 10.1103/PhysRevB.98.054108

I. INTRODUCTION

Defects and dopants have critical impacts on semiconductor material properties and applications. For example in photovoltaics (PV), defect-mediated recombination limits the lifetime of photogenerated minority carriers resulting in decreased open-circuit voltage and efficiency [1–6]. The detrimental or beneficial impacts vary with defect properties such as formation and transition energies [7–9]. Yet, it is often very difficult to measure these properties experimentally even with multiple techniques. Consequently, first-principles calculations have played a very important role in calculating defect properties, both complementing experimental results and serving as a powerful method to scientifically understand, predict, and manipulate defects and material properties.

However, the accurate prediction of defect properties can be challenging and often depends on details in the approach, such as the choice of the functional and the inclusion of spin-orbit coupling (SOC). Standard density-functional theory (DFT) calculations, e.g., with generalized gradient approximation (GGA) [10], often underestimate the band gap [11] and overdelocalize defect states [12–14], which affects the calculated defect properties. For some systems, even when the band gap from DFT-GGA calculations agrees with experiment, the positions of the band edges with respect to the defect transition levels can still be incorrect [15]. Hybrid functionals serve as an alternative to tackle these electronic band-structure problems by introducing a certain amount of exact Hartree-Fock (HF) exchange energy into the standard DFT functional to cancel the residual self-interaction error. For semiconductors with heavy elements, e.g., tellurium (Te) and lead (Pb), the inclusion of spin-orbit coupling becomes important and can significantly influence the band structure and defect properties by either shifting the band edges [15–17] or splitting defect states [18]. In the literature, this brings the calculated results into qualitative agreement with experiments. For example, West *et al.* demonstrated that Bi_2Se_3 can be predicted as native n type (instead of native p type without SOC) due to the shift of band edges induced by SOC, and that the Bi_{Se} defect changes from acceptor type without SOC to donor type with SOC [16]. Du reported that the combination of both using a hybrid functional and including SOC is necessary to obtain the correct edge positions in lead iodide perovskites for a defect picture in agreement with experiments [15]. These examples show that reproducing a realistic host band structure by including SOC and carefully tuning the hybrid functional parameters can be necessary for obtaining reliable defect properties, i.e., formation and transition energies, more in alignment with experimental results. It is often tacitly assumed that it is also a sufficient condition, but this is ultimately an open question.

Cadmium telluride (CdTe) is an ideal material system to explore this question. CdTe is a leading thin-film solar absorber material in the PV industry with many advantages, such as an ideal 1.5-eV band gap and high absorption coefficient [19,20]. First Solar has achieved the world-record CdTe solar power conversion efficiency of 22.1%, and this technology is

*Jie.Pan@NREL.gov
†Stephan.Lany@NREL.gov

providing electricity at costs competitive with conventional fuels today [21]. However, the CdTe properties still have headroom for further improvement. Polycrystalline CdTe is deposited quickly and followed by $CdCl_2$ and Cu exposure to make complete solar cells [22–26]. However, significant self-compensation leads to a limitation of the hole density to about $10^{14}\,cm^{-3}$, and recombination losses remain an important problem; both issues limit the performance [27,28]. According to the Shockley-Read-Hall theory, deep-level defects can act as nonradiative recombination centers by assisting the coupling of the photogenerated carriers [1,2], and thus, limiting the open-circuit voltage and fill factor [19]. As a result, the accurate determination of defect levels with respect to the band edges is very critical for both device modeling and experiments to further improve the performance. Recently, standard hybrid functional calculations without SOC have been employed to predict CdTe bulk and defect properties [19,29–31]. However, strong SOC effects in the Te-p shell are known to play an important role for the band structure of tellurides [16] and have been qualitatively discussed for the $(0/-)$ transition level of Cd vacancy in CdTe [32]. As a result, the formation energies of fully ionized defects are expected to change in accordance with the valence-band-edge shift caused by SOC [33]. In addition, SOC can further split defect states, thereby affecting the transition energies between different charge states.

In this paper, we use CdTe as an example to address the coupled effects of the SOC and band-gap corrections via hybrid functionals on the prediction of defect properties. Hybrid functional parameters are chosen to reproduce the experimental CdTe band gap when the SOC is included. We further investigate the SOC effect on predicting the defect formation energy and transition energy with this band-gap-corrected hybrid functional. For the effect of SOC on transition energies, we use the Cd interstitial (Cd_i) and the A-center ($Cl_{Te} - V_{Cd}$ defect pair) as examples of defect states that are indirectly (Cd-s-like state) or directly (Te-p-like state) affected by SOC, respectively. We further simulate the defect equilibrium in intrinsic CdTe and discuss the effect of SOC on net carrier concentrations.

II. METHODS

The energies and electronic density of states were calculated using the Vienna *Ab initio* Simulation Package (VASP) with the projector-augmented-wave implementations for DFT [34], hybrid functionals [35], and spin-orbit coupling [36]. The bulk/defect supercells were relaxed with a cutoff energy of 330 eV for the plane-wave basis sets, a $2 \times 2 \times 2$ gamma k-point mesh. The convergence criteria are total energy difference below 10^{-4} eV per supercell for electronic relaxation and total force below 0.02 eV/Å on each atom for ionic relaxation. The CdTe crystal has the zinc blende structure (space group: $F\bar{4}3m$, No. 216) and a 64-atom simple cubic supercell was constructed for defect calculations. For the exchange and correlation in density-functional theory, we used the GGA in the revised Perdew-Burke-Ernzerhof form for solids (PBEsol) [37]. Hybrid functional calculations were performed using the range-separated form of the Heyd-Scuseria-Ernzerhof (HSE06) functional [38]. The q-point grid representation of the Fock exchange was uniformly reduced by a factor of 2 (NKRED = 2) to save computational cost. The occupancies in hybrid functional defect calculations with NKRED = 2 were carefully checked to ensure that no partial occupancies occur.

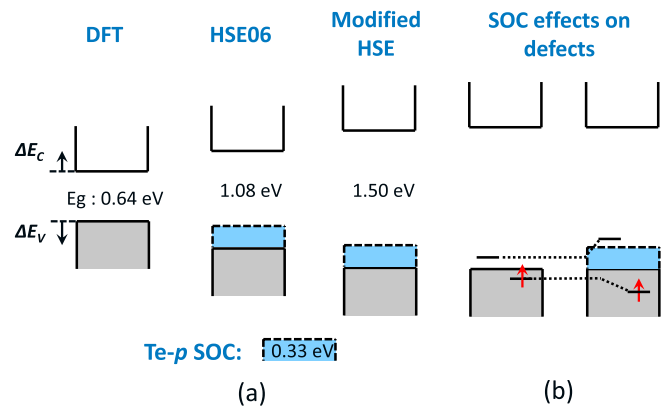

FIG. 1. (a) Values of band gap calculated from different calculations: standard DFT, HSE06 with SOC, and modified HSE (33% HF exchange) with SOC. (b) Schematic illustration of the SOC effect on the predicted electronic structure of an open-shell defect.

Standard DFT has a notorious problem of underestimating material band gaps. For example, the CdTe band gap from standard DFT is about 0.64 eV, as compared to the experimental room-temperature band gap of 1.5 eV [39]. The hybrid functional can alleviate this problem by mixing a certain amount of HF exchange into the GGA functional. The standard hybrid functional (HSE06, 25% Fock exchange) gives a band-gap value for CdTe of about 1.41 eV [Fig. 1(a)]. However, heavy Te atoms in CdTe experience a strong SOC effect, which brings the valence-band maximum (VBM) up by about 0.33 eV [Fig. 1(a)]. This effect reduces the band gap relative to an HSE06 calculation without SOC, implying that HSE06 significantly underestimates the band gap. In order to have a corrected band gap close to the experimental value, in this study we used a modified hybrid functional with 33% Fock exchange. This choice gives about a 1.50-eV band gap including the SOC effects [Fig. 1(a)]. In addition, the use of the PBEsol parametrization for the GGA allows us to get a lattice constant of about 6.48 Å. The lattice constant in this functional is very close to the experimental value [40], and should improve the defect predictions that are sensitive to the lattice parameters, which is especially the case for defects with large relaxations.

Another problem associated with standard DFT is its failure, even qualitatively, to describe the symmetry-broken defect states resulting in partial occupancies instead of the physically correct splitting into fully occupied and empty states [41]. Because of the complex energy surface due to Jahn-Teller distortions [41,42], this additional complexity due to electronic correlations often leads to multiple locally stable configurations for open-shell defects. Coupled with the higher computational cost of the hybrid functionals, a complete sampling of the configurations space within hybrid functional calculations becomes very tedious. To overcome this challenge, we employed a GGA+U+V functional to effectively sample different configurations. Here, U is the standard DFT+U potential [43], and V is a nonlocal external potential [44]. The U/V parameters [45] were chosen to approximately correct both the band gap and the non-Koopmans behavior of standard DFT, and to

stabilize symmetry-broken solutions [41]. This method allows us to obtain a solution with appropriate electronic and atomic symmetries at the cost of a standard DFT calculation. For quantitative energies, we feed the most likely solutions into subsequent HSE calculations, which usually converge quickly from this starting point.

With the corrected bulk properties and efficient defect configuration sampling, the formation energy of each defect is calculated by

$$\Delta H_f(q) = E(q) - E(\mathrm{CdTe}) - \sum n_i\left(\mu_i^0 + \Delta\mu_i\right) + q(E_F + E_V), \quad (1)$$

where $E(q)$ and $E(\mathrm{CdTe})$ are the ground-state energies calculated from DFT for a defect supercell with charge q and a perfect supercell. Here, n_i is defined as the difference of the atom numbers between the imperfect and perfect supercells, and μ_i^0 are the reference energies for the elements in their standard state. For each element $\Delta\mu_i$ is the chemical potential referenced to the elemental energies, and E_F is the electronic Fermi level referenced to the bulk VBM (E_V). For defect formation energies, potential alignment and image charge corrections have been included as described in Ref. [44]. The potential alignment was also taken into account for single-particle energy spectra, i.e., the defect projected density of states (DOS), both for neutral and charged states, to ensure the correct lineup with respect to the host band structure. Additionally, image potential corrections were applied to single-particle energies for charged defect states as described in Ref. [46]. The defect transition energy $\varepsilon(q/q')$ between charge state q and q' can be calculated by

$$\varepsilon(q/q') = [\Delta H_f(q) - \Delta H_f(q')]/(q' - q). \quad (2)$$

To improve the description of the chemical potential ranges, we used the fitted elemental-phase reference energies (FERE) [47]. This approach was designed to improve upon the incomplete error cancellation in DFT when energy differences are taken between different types of matter (insulators, metals, and molecules). This approach is also suitable for hybrid functional calculations [33], where the mixing parameter used for the compound (CdTe) phase is not well justified for the elements involved in the studied defects (here, Cd, Te, Cl). To determine FERE energies, we performed a fit for 23 different compounds in the modified HSE functional, based on tabulated experimental enthalpies of formation [48,49]. The resulting FERE energies and enthalpies of formation are given in Supplemental Material [45].

III. RESULTS AND DISCUSSION

A. SOC effects on formation energies

The SOC effect influences the band-edge energies. For example, the VBM shifts up by about 0.33 eV, and this can affect the formation energies and resulting defect populations. In the case of fully ionized defects that involve only closed-shell atomic orbital configurations (e.g., Te-p^6 for V_{Cd}^{2-} or Cl-p^6 for $\mathrm{Cl}_{\mathrm{Te}}^{+}$), the SOC effects on defect formation energies can be included by a simple VBM shift on top of a non-SOC calculation [15]. This is because the SOC splits the atomic orbital energies such that the average orbital energy is approximately preserved. Hence, for a closed-shell orbital occupation, the direct energy contribution due to the splitting is small. The remaining dominant SOC effect is the shift of the band-edge energies, which enters the formation energy for charged defects by defining the bounds for E_{F} [see Eq. (1)]. In the case of open-shell defect states, e.g., Te-p^5 in $(\mathrm{Cl}_{\mathrm{Te}} - V_{\mathrm{Cd}})^0$ discussed below, there can be an energy gain associated with the orbital splitting by SOC. Here, it is important to include SOC in the defect supercell calculation for accurate defect calculation of levels. Furthermore, regarding the thermochemical properties, which define the bounds for the chemical potentials, the energy changes due to SOC are approximately a constant energy contribution for each atom [47]. Such atomic energy changes cancel upon taking energy differences that observe the particle conservation, and therefore do not affect the compound formation enthalpies.

Figure 2 shows the defect formation energies of fully ionized defects in Te- and Cd-rich conditions, respectively. In the Te-rich condition ($\Delta\mu_{\mathrm{Te}} = 0$ eV), the Cu and Cl chemical potential are chosen as $\Delta\mu_{\mathrm{Te}} + \Delta\mu_{\mathrm{Cu}} = \Delta H(\mathrm{CuTe})$ and $3\Delta\mu_{\mathrm{Cd}} + 2\Delta\mu_{\mathrm{Cl}} + 2\Delta\mu_{\mathrm{O}} = \Delta H(\mathrm{Cd_3Cl_2O_2})$. In the Cd-rich condition ($\Delta\mu_{\mathrm{Cd}} = 0$ eV), the Cu and Cl chemical potential are chosen as $\Delta\mu_{\mathrm{Cu}} = 0$ eV (elemental Cu) and $3\Delta\mu_{\mathrm{Cd}} + 2\Delta\mu_{\mathrm{Cl}} + 2\Delta\mu_{O} = \Delta H(\mathrm{Cd_3Cl_2O_2})$. The chemical potential of oxygen ($\Delta\mu_{\mathrm{O}} = -0.81$ eV) is the chemical potential of oxygen gas at 450 °C in air (0.2 atm $p_{\mathrm{O_2}}$). These conditions correspond to typical processing protocols for a $CdCl_2$ treatment [50,51]. Note that the $Cd_3Cl_2O_2$ phase imposes a tighter constraint to $\Delta\mu_{\mathrm{Cl}}$ than $CdCl_2$, thereby supporting the conclusion of Ref. [52] that this ternary phase acts as the major chlorine-containing component under the actual process conditions.

We now compare the present results using the band gap and SOC-corrected functional with previous hybrid-functional-based calculations [29,31,53]. Under the Te-rich condition, $\mathrm{Cl}_{\mathrm{Te}}^{+}$ has a lower formation energy than that of V_{Te}^{2+} across the whole band-gap region, in agreement with Ref. [31]. However, in Ref. [29], the formation energy of $\mathrm{Cl}_{\mathrm{Te}}^{+}$ can be higher than that of V_{Te}^{2+} near the VBM under the same growth condition. This cannot be explained by the choice of $\Delta\mu_{\mathrm{Cl}}$, since Ref. [29] used a higher chemical potential value for $\Delta\mu_{\mathrm{Cl}}$ than that used here. The discrepancy can be attributed to the band-edge shift caused by the choice of hybrid functional with a larger HF fraction and the inclusion of SOC. This band-edge shift effect is also reflected in the crossing point of $\mathrm{Cu_i^{+}}$ and $\mathrm{Cd_i^{2+}}$. Under the Cd-rich condition, the crossing point in our calculation is closer to the VBM relative to Ref. [29], in which the crossing point is near the conduction band minimum (CBM). We also find that the Cd interstitial $\mathrm{Cd_i^{2+}}$ is lower in energy than the charged Te vacancy V_{Te}^{2+}, in contrast to Ref. [53], but in agreement with Ref. [31]. Since both defects have the same dependence on chemical potentials and E_{F}, the energy ordering discrepancy is not explained by the FERE, band gap, and SOC corrections.

The results demonstrate that the inclusion of the SOC in the hybrid functional calculation can potentially change defect formation energies, and thus their relative populations, importance, doping, and recombination properties. For example, for p-type CdTe under Te-rich conditions, the majority defects are $\mathrm{Cu_i}$, $\mathrm{Cu_{Cd}}$, $\mathrm{Cl_{Te}}$, and $\mathrm{Cd_i}$ with SOC. The $\mathrm{Te_{Cd}}$ antisite has been considered an important recombination center in p-type CdTe [54]. However, in the present study, the formation energy of

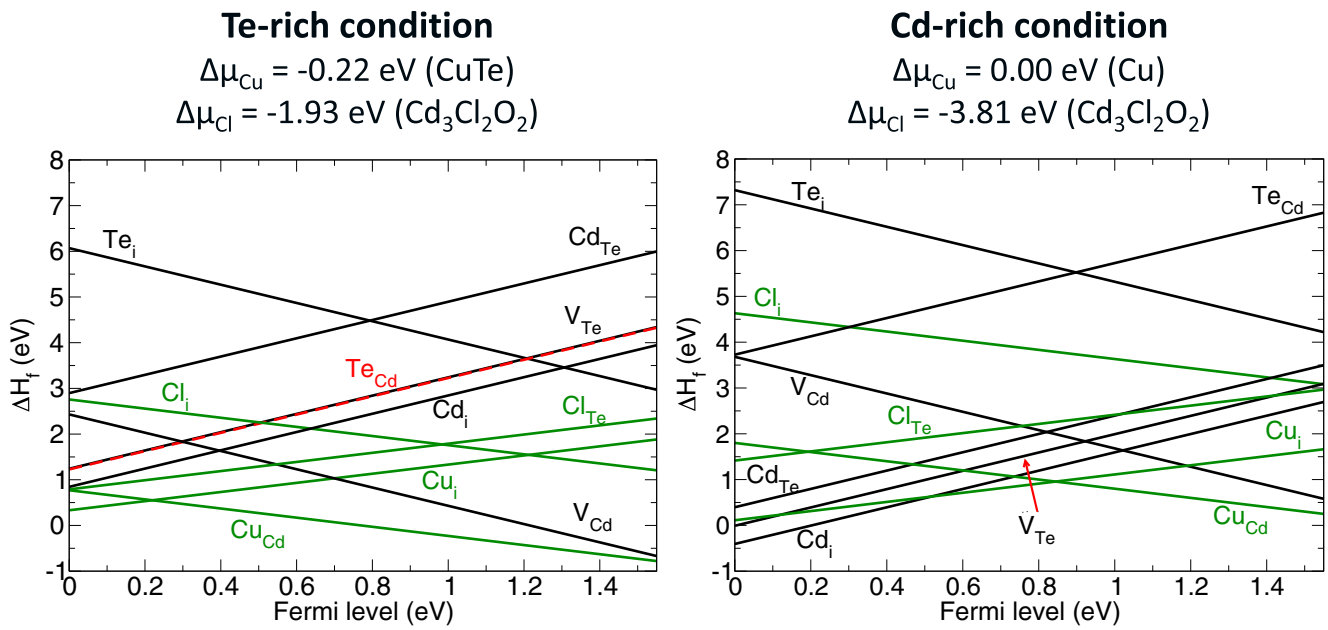

FIG. 2. Formation energies of fully ionized defects in CdTe under a Te-rich condition and a Cd-rich condition, calculated using the HSE06 hybrid functional with 33% Hartree-Fock exchange, and including the VBM shift due to SOC.

Te_{Cd}^{2+} has been raised due to the SOC-induced VBM upshift. In addition, the Te_{Cd}^{2+} formation energy is always higher than Cd_i. In the past, Cd_i has often been considered as a benign defect with shallow donor levels. But due to its low formation energy, and the larger band gap in our computational approach, we performed a more detailed study of the nonradiative recombination mechanism for Cd_i (see Sec. III B 1).

B. SOC effects on transition levels

The way in which SOC can affect defect states that are not fully ionized depends on the electronic structure of the defect. Generally speaking, the molecular orbitals corresponding to a defect state split due to the crystal-field symmetries and the Coulomb correlation, thereby separating occupied and unoccupied quasiparticle energies [41]. Since SOC causes an additional splitting, it can be expected that the defect transition levels become deeper, as illustrated in Fig. 1(b), when viewed relative to a fixed energy reference, such as the average electrostatic potential. On the other hand, the VBM upshift reduces the distance of the unoccupied state from the VBM, which makes acceptor states shallower. The final defect-level position depends on the balance between these two effects. This balance can have a particularly strong influence on the defect transition for relatively shallow acceptor states close to the VBM, as illustrated in Fig. 1(b). In the following, we investigate in more detail the transition energies of the Cd interstitial and the Cl *A* center [55], a $Cl_{Te} - V_{Cd}$ defect pair between a Cd vacancy and a substitutional Cl donor. The *A*-center acceptor level has been experimentally established, allowing for a direct comparison with calculated values.

1. Cadmium interstitials

The Cd interstitial (Cd_i) is an important intrinsic defect with low formation energy near the VBM [29,31,53]. As shown in Figs. 3(a) and 4, a Cd atom can be located at the interstitial site that is tetrahedrally coordinated by four Te atoms [Cd_i(Te)], or at the Cd-coordinated site [Cd_i(Cd)]. Interestingly, the site preference of Cd_i depends on the charge state. In the 2+ charge state, the Cd_i(Te) configuration is lower in energy, but in the neutral state, the Cd_i(Cd) structure is energetically favored. Both defect structures produce a state inside the band gap. The Cd_i(Cd) creates a deeper donor level with the overall (2+/0) transition at $E_{CBM}-0.45$ eV [Fig. 3(d)]. Thus, here the fully band-gap-corrected hybrid functional with SOC indicates that Cd interstitials produce a deeper level than found in previous calculations based on DFT or the standard HSE06 functional [29–31,53]. This implies the Cd_i defect could act as an electron trap and its role as a potential recombination center has been underappreciated.

To test the sensitivity of the defect properties on the details of the hybrid functional and SOC, we show in Fig. 3(d) the position of the $\varepsilon(2+/0)$ level (average between first and second ionization levels) for the Cd_i(Cd) defect as a function of the Fock exchange parameter, both with and without SOC. Several observations are notable. First, the transition level stays almost constant on an absolute scale (approximated by using the average electrostatic potential as reference), while the band gap opens more or less symmetrically in the conduction and valence bands. This behavior is often observed for deep levels [56]. Second, the magnitude of the VBM shift due to SOC is not sensitive to the mixing parameter. ΔE_v^{soc} varies only between 0.316 eV and 0.355 eV for $\alpha = 0.2$ and $\alpha = 0.5$, respectively. As expected from the $l = 0$ angular momentum character, the CBM is virtually unaffected by SOC, with changes less than 0.037 eV. Similarly, the distance of the Cd_i level to the conduction band is not affected by the SOC since it also has an $l = 0$ character. Thus, the deep Cd_i state compared to previous calculations is a result only indirectly related to SOC, in that a larger Fock parameter α is needed to reconcile the experimental

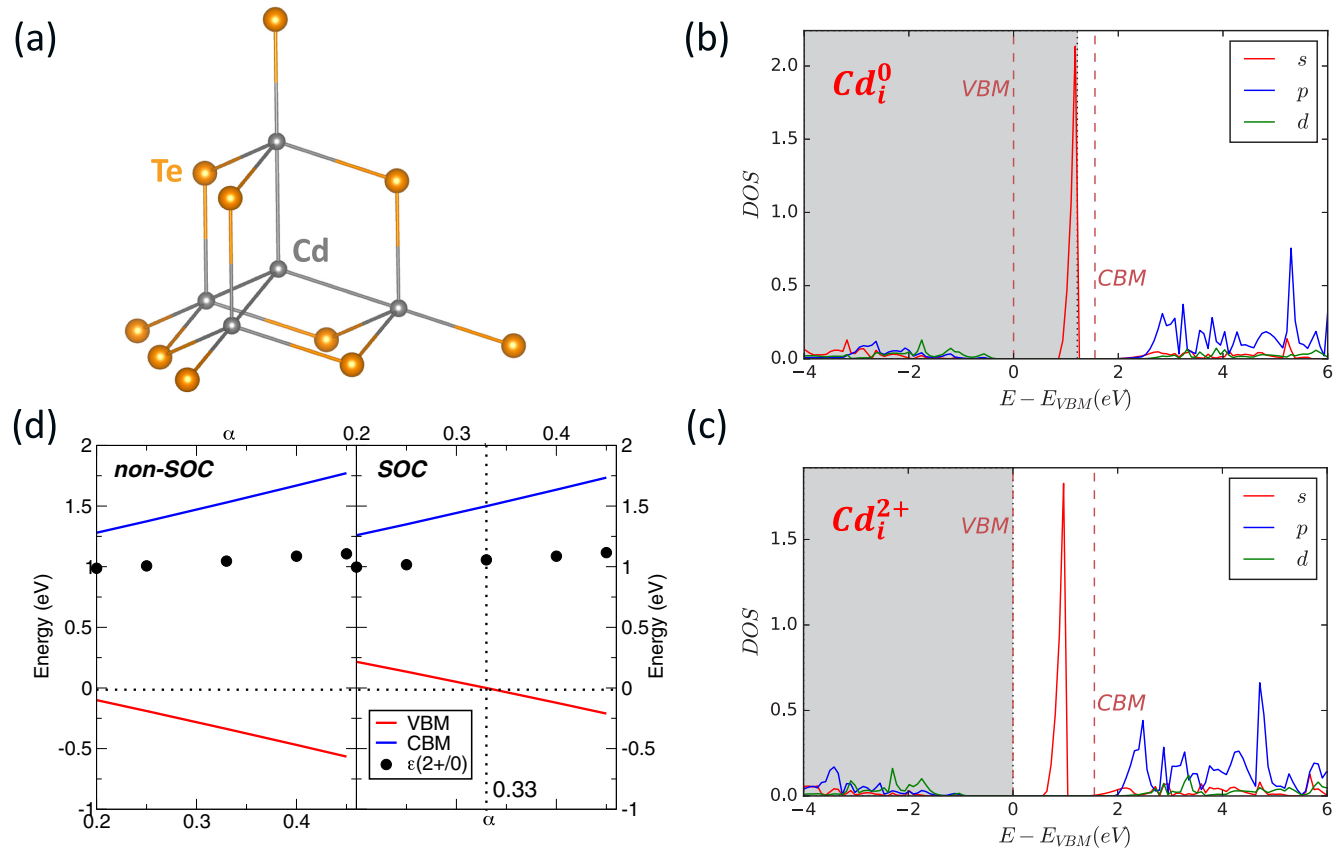

FIG. 3. (a) Defect structure of Cd_i tetrahedrally bonded with four nearby Cd ions. (b) Defect site projected DOS of Cd_i(Cd) in the neutral state and (c) in the 2+ state. The energy range of occupied states is indicated by the gray shading. The DOS in (b) and (c) were calculated from non-SOC HSE calculations ($\alpha = 0.33$), but the SOC effect on the VBM energy was included. (d) Band edges and $\varepsilon(2+/0)$ transition levels for Cd_i, determined with and without SOC, as a function of the hybrid functional mixing parameter.

band gap when SOC is included. It must be noted, however, that the deep and localized character of Cd_i is maintained even for smaller values of α down to 0.2 [cf. Fig. 3(d)] and below, implying that its role as a potential recombination center is robust against α variation.

The behavior of a defect as a recombination center depends also on the location of the defect states. Transition levels in the vicinity of the CBM can indicate either a shallow delocalized effective mass state, or a localized deep level that coincidentally occurs close to the band edge. Our calculated defect DOS, presented in Figs. 3(b) and 3(c), show that Cd_i clearly produces a localized quasiparticle state inside the gap, separated from the continuum of conduction-band states. We now discuss the electron capture mechanism involving this defect state. As shown in Fig. 4, in p-type CdTe (E_F close to VBM), the interstitial Cd prefers to stay at the Te-neighbored site forming Cd_i^{2+}(Te), which has its unoccupied defect state right below the CBM [45]. This empty state can capture a free electron which is the minority carrier in p-type CdTe and becomes Cd_i^{+}(Te). However, Cd_i^{+}(Te) is thermodynamically unstable and can relax to the more stable Cd_i^{+}(Cd) configuration (black arrow in Fig. 4), which is a spin-polarized defect with one occupied state in the middle of the band gap and the other empty state right below the CBM [45]. The unoccupied state can further bind a second free electron, resulting in the neutral Cd_i^{0}(Cd) defect. Thus, the capture of two minority carriers can be summarized as a three-step process,

$$Cd_i^{2+}(\text{Te}) \xrightarrow{+e} Cd_i^{+}(\text{Te}) \xrightarrow{\text{Relax}} Cd_i^{+}(\text{Cd}) \xrightarrow{+e} Cd_i^{0}(\text{Cd}). \quad (3)$$

The first capture corresponds to the (2+/+) transition of Cd_i(Te) at $E_{CBM} - 0.21$ eV. The second step is an activated structural relaxation with an energy barrier of $\Delta E_b =$

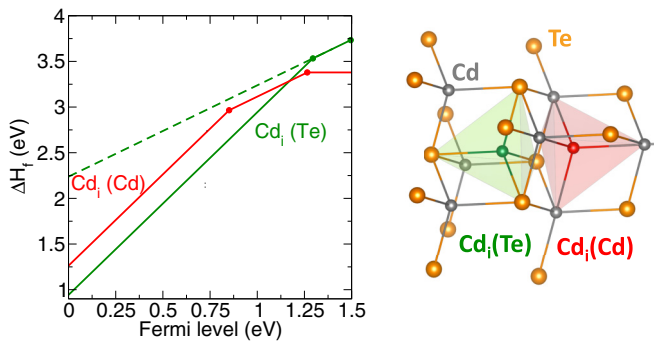

FIG. 4. Left: Transition energies $\varepsilon(2+/+)$ and $\varepsilon(+/0)$ for the two structural configurations of Cd_i calculated from non-SOC HSE calculations ($\alpha = 0.33$), but the SOC-induced shift of the VBM energy is included (ΔH_f shown for Te-rich condition). Right: Atomic structures of Cd interstitial [Cd_i(Te)] surrounded by four Te atoms and Cd interstitial [Cd_i(Cd)] surrounded by four Cd atoms.

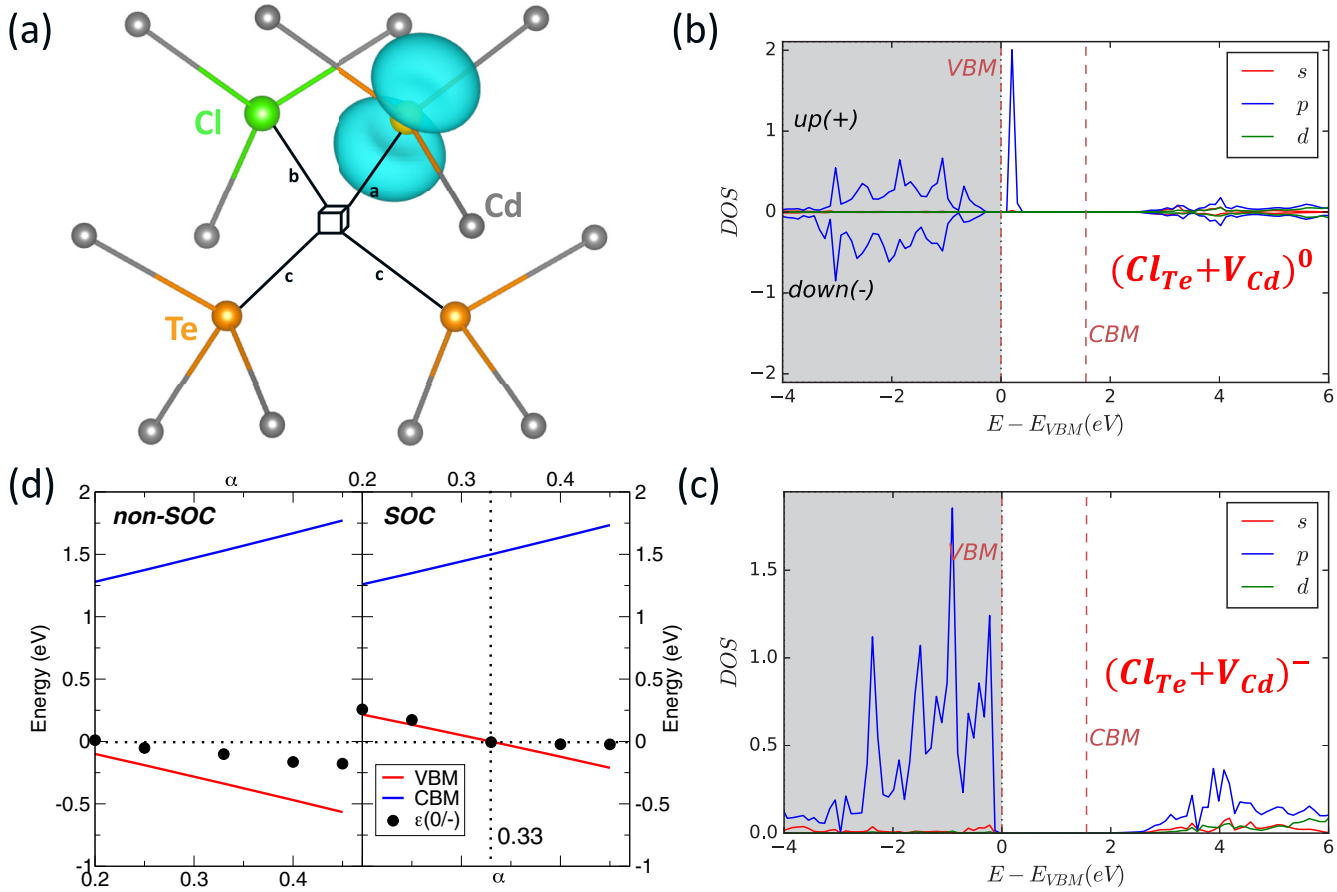

FIG. 5. (a) Atomic structure of the charge-neutral A center in C_{1h} symmetry (distances from V_{Cd} site: $a = 2.95$ Å, $b = 3.26$ Å, and $c = 2.44$ Å), showing also the magnetization density with an isosurface density of 0.01 e/Å^3 (spin-polarized calculation without SOC). (b) Defect site projected DOS on the Te atom with the bound hole in the neutral state and (c) in the 1− charge state of the A center. The DOS in (b) and (c) were calculated from non-SOC HSE calculations ($\alpha = 0.33$), but the SOC effect on the VBM energy was included. (d) Band edges and $\varepsilon(0/-)$ transition level for ($Cl_{Te} - V_{Cd}$), determined with and without SOC, as a function of the hybrid functional mixing parameter.

0.33 eV, and an associated lifetime of 10^{-7}–10^{-8} s [$\tau \approx \nu_{ph}{}^{-1}\exp(\Delta E_b/kT)$, where ν_{ph} is the average phonon frequency, typically 10^{12}–10^{13} s^{-1}] [57]. The third step is the electron capture due to the (+/0) transition of Cd_i(Cd) at $E_{CBM} - 0.24$ eV.

2. *The* $Cl_{Te} - V_{Cd}$ *defect pair (Cl A center)*

The Cl A center is an ideal defect for the study of the SOC effect on the transition levels of a shallow acceptor state with a similar atomic orbital character (Te-p) as the VBM. This defect is considered critical in detector and PV applications because it offers an explanation for how Cl, which would be a donor on a Te site, contributes to p-type doping. In addition, the acceptor ionization energy, i.e., the $\varepsilon(0/-)$ transition level, is experimentally known to be 120 ± 3 meV above the VBM [55]. In the charge-neutral $(Cl_{Te} - V_{Cd})^0$ state, a hole is bound at one of the three Te neighbors surrounding the V_{Cd} site. Obtaining the correct localization behavior requires using a post-DFT functional that corrects the correlation effects for open-shell defect states [41]. Figure 5(a) shows the symmetry-broken atomic structure of a neutral A center with a C_{1h} symmetry, where the Te atom with the bound hole relaxes much farther away from the V_{Cd} site than the remaining two Te atoms. The localized hole state is visualized in Fig. 5(a) by the magnetization density, i.e., the difference between spin-up and spin-down densities obtained from a non-SOC calculation. The corresponding quasiparticle hole state is seen as a Te-p-like, unoccupied narrow peak in the density of states [Fig. 5(b)]. In the negatively charged $(Cl_{Te} - V_{Cd})^-$ state, all valence-band-derived states are occupied, and the A center assumes the C_{3v} symmetry expected from the atomic lattice decoration.

The acceptor binding energy, i.e., the $\varepsilon(0/-)$ transition energy, depends crucially on the hybrid functional parameter α, controlling the energy splitting between occupied and unoccupied states due to correlation effects [41]. As expected, the acceptor level moves monotonically deeper into the band gap with increasing α, as shown in Fig. 5(d). At $\alpha = 0.33$, the value that reproduces the experimental band gap, the $\varepsilon(0/-)$ lies at 0.236 eV above the VBM (excluding SOC), somewhat deeper than the experimental value of 0.120 eV. Unlike the case of the Cd_i, where the SOC effect was essentially captured by adding the SOC-induced VBM shift to E_V, the effect on the A-center level is more subtle. At small values of α (e.g., $\alpha = 0.25$), the

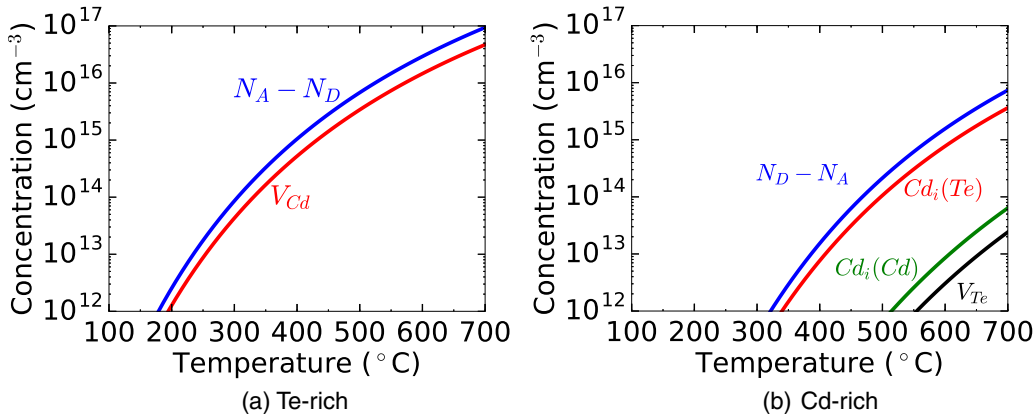

FIG. 6. Net doping and major defect concentration as a function of temperature: (a) Te-rich condition ($\Delta\mu_{\mathrm{Cd}} = -1.25$ eV and $\Delta\mu_{\mathrm{Te}} = 0$ eV) and (b) Cd-rich condition ($\Delta\mu_{\mathrm{Cd}} = 0$ eV and $\Delta\mu_{\mathrm{Te}} = -1.25$ eV).

VBM shift is large enough to overcome the localization energy of the acceptor state, so that the hole becomes a delocalized effective mass state. After correction for band-filling effects [58], the $\varepsilon(0/-)$ level coincides with the VBM. Only at values of α larger than 0.33, the localized acceptor level separates again from the valence band, and then further deepens with increasing α as in the case of the non-SOC calculations. It now becomes obvious that the SOC-induced shift of the occupied VBM states is significantly larger than that of the unoccupied hole state of the A-center acceptor, even though both are predominantly formed by Te-p states. A value above $\alpha = 0.4$ is needed to bring the A-center acceptor level in agreement with the experimental value of 120 meV. At this large fraction of Fock exchange, however, the band gap is already overestimated ($E_{\mathrm{g}} = 1.76$ eV), and this value is also much larger than the standard value $\alpha = 0.25$ of the popular HSE06 functional. Thus, a fully consistent description within the hybrid functional approach remains elusive, but the parameter of $\alpha = 0.33$ used here for the absolute defect formation energies (see Sec. III A) should considerably improve estimates relative to the standard $\alpha = 0.25$ HSE functional.

3. Carrier concentration

Based on the defect formation energies, we performed thermodynamic simulations [59–61] to calculate the defect and carrier concentrations. Results are shown in Fig. 6 for the intrinsic case without dopants. Both anion and cation defects, such as interstitials, vacancies, and antisites, were included in the simulation; however, the Te interstitial was excluded because it has a high formation energy across the whole Fermi energy range (see Fig. 2). Both Cd interstitial sites discussed in Sec. III B 1 were considered. Intrinsic CdTe can be either p type or n type depending on the growth conditions. As shown in Fig. 6, under the Te-rich condition, CdTe is p type due to the formation of the V_{Cd} acceptor, but under the Cd-rich condition, CdTe can be slightly n type at elevated temperatures with $\mathrm{Cd_i}$(Te) as the main donor. The calculated net doping level under the Te-rich condition is about $10^{14}\,\mathrm{cm^{-3}}$ at 330 °C and about $10^{17}\,\mathrm{cm^{-3}}$ at 700 °C. This agrees well with experimentally measured values under Te-rich conditions [39,62]. However, it is one order of magnitude higher (about $10^{16}\,\mathrm{cm^{-3}}$ at 800 K or 527 °C) than the value obtained from defect simulations without the SOC effect included (about $10^{15}\,\mathrm{cm^{-3}}$ at 800 K [19]). In addition, under the Cd-rich condition, the net doping (n type) from our calculation is lower than Ref. [19] at 800 K. In Ref. [19], the major donor under the Cd-rich condition was believed to be V_{Te}. However, after the inclusion of the SOC effect on VBM in our calculation, the major donor is $\mathrm{Cd_i}$ neighbored by four Te atoms [Fig. 6(b)]. This is caused by (1) V_{Te} in our calculation turning out to be a deep-level defect [45]; (2) as discussed in Sec. III B 1, $\mathrm{Cd_i^{2+}}$ has a lower formation energy value compared with that of V_{Te}^{2+}. In summary, the inclusion of SOC can change the defect equilibrium and further influence the carrier concentration and net doping levels. Specifically, in the example of CdTe, the inclusion of SOC makes the calculated equilibrated net doping levels at elevated temperatures more aligned with experimentally measured values, such as the net doping in the Te-rich condition, and shifts the predicted major donor from the previously reported Te vacancy [19] to the Cd interstitial.

IV. CONCLUSION

The results demonstrate that the inclusion of SOC in band-gap-corrected hybrid functional calculations has a significant impact on predicted defect properties, populations, doping, and recombination. The standard hybrid functional (HSE06) underestimates the CdTe band gap once SOC is included, and an increase of Fock exchange mixing ($\alpha = 0.33$) is needed to achieve the correct band gap value. The PBEsol functional provides an accurate value of lattice constant, which can be important for the calculation of defects with large lattice relaxations. The influence of SOC to the formation energy of closed-shell (fully ionized) defects is dominated by the valence-band-edge shifts due to SOC (0.33-eV upward shift). Similarly, defect levels such as that of $\mathrm{Cd_i}$ (Cd-s-like) that are not directly affected by SOC can be described by simply adding the band-edge shift to a non-SOC calculation. For defect states such as that of the $\mathrm{Cl_{Te}} - V_{\mathrm{Cd}}$ pair (Te-p-like) that are formed by orbitals subject to SOC, the final transition level depends on the balance between the SOC effects on the band edge and on the defect state. We find here that for the exchange parameter

optimized for the band gap, the acceptor state is still too shallow compared to the available experimental data.

The predictions for the intrinsic doping and for recombination centers also vary significantly with the SOC inclusion. The formation energy of the Te_{Cd} recombination site is increased with SOC, lowering its equilibrium concentrations. In our calculations, the dominant donor-type defect is the Cd_i defect, which has a somewhat lower formation energy than the V_{Te} defect. An important implication for PV is our finding that the Cd_i defect forms a localized deep level more than 0.2 eV below the conduction band and can trap up to two electrons via a phonon-mediated change of the interstitial site. This finding suggests that the impact of Cd_i should not be discounted as a benign shallow defect. Overall, our results demonstrate how spin-orbit effects in combination with band-gap corrections affect the defect physics of PV materials with heavy elements, such as CdTe, and these insights also apply to many other material systems.

ACKNOWLEDGMENTS

This work was supported by the US Department of Energy (DOE) under Contract No. DEAC36-08GO28308 with the Alliance for Sustainable Energy, LLC, the manager and operator of the National Renewable Energy Laboratory (NREL). The funding was provided by the Office of Energy Efficiency and Renewable Energy (EERE), Solar Energy Technology Office, within the SunShot program, Award No. DE-EE0006344. This work used high-performance computing resources located at the NREL and sponsored by DOE-EERE. The views expressed in the article do not necessarily represent the views of the DOE or the U.S. Government. The U.S. Government retains and the publisher, by accepting the article for publication, acknowledges that the U.S. Government retains a nonexclusive, paid-up, irrevocable, worldwide license to publish or reproduce the published form of this work, or allow others to do so, for U.S. Government purposes.

[1] W. Shockley and W. T. Read, Phys. Rev. **87**, 835 (1952).
[2] R. N. Hall, Phys. Rev. **87**, 387 (1952).
[3] L. Shi and L. W. Wang, Phys. Rev. Lett. **109**, 245501 (2012).
[4] A. Alkauskas, Q. Yan, and C. G. Van de Walle, Phys. Rev. B **90**, 075202 (2014).
[5] A. M. Stoneham, Rep. Prog. Phys. **44**, 1251 (1981).
[6] X. Chen, H. Lu, Y. Yang, and M. C. Beard, J. Phys. Chem. Lett. **9**, 2595 (2018).
[7] S.-H. Wei, Comput. Mater. Sci. **30**, 337 (2004).
[8] C. G. Van de Walle and J. Neugebauer, J. Appl. Phys. **95**, 3851 (2004).
[9] C. Freysoldt, B. Grabowski, T. Hickel, J. Neugebauer, G. Kresse, A. Janotti, and C. G. Van de Walle, Rev. Mod. Phys. **86**, 253 (2014).
[10] J. P. Perdew, K. Burke, and M. Ernzerhof, Phys. Rev. Lett. **77**, 3865 (1996).
[11] D. R. Hamann, Phys. Rev. Lett. **42**, 662 (1979).
[12] S. Lany and A. Zunger, Phys. Rev. B **80**, 085202 (2009).
[13] M. d'Avezac, M. Calandra, and F. Mauri, Phys. Rev. B **71**, 205210 (2005).
[14] A. Droghetti, C. D. Pemmaraju, and S. Sanvito, Phys. Rev. B **78**, 140404(R) (2008).
[15] M. H. Du, J. Phys. Chem. Lett. **6**, 1461 (2015).
[16] D. West, Y. Y. Sun, H. Wang, J. Bang, and S. B. Zhang, Phys. Rev. B **86**, 121201(R) (2012).
[17] Z. G. Yu and Y.-W. Zhang, Phys. Rev. B **94**, 195206 (2016).
[18] W.-F. Li, C. Fang, and M. A. van Huis, Phys. Rev. B **94**, 195425 (2016).
[19] J.-H. Yang, W.-J. Yin, J.-S. Park, J. Ma, and S.-H. Wei, Semicond. Sci. Technol. **31**, 083002 (2016).
[20] J. J. Loferski, J. Appl. Phys. **27**, 777 (1956).
[21] First Solar Achieves Yet Another Cell Conversion Efficiency World Record (First Solar News Release) http://investor.firstsolar.com/news-releases/news-release-details/first-solar-achieves-yet-another-cell-conversion-efficiency.
[22] X. Wu, Sol. Energy **77**, 803 (2004).
[23] A. Luque and S. Hegedus, *Handbook of Photovoltaic Science and Engineering*, 2nd ed. (John Wiley and Sons, New York, 2011), Chap. 13, 14.
[24] M. Amarasinghe *et al.*, Adv. Energy Mater. **8**, 1702666 (2018).
[25] N. R. Paudel, C. R. Grice, C. Xiao, and Y. Yan, J. Mater. Sci.: Mater. Electron. **26**, 4708 (2015).
[26] N. R. Paudel, C. Xiao, and Y. Yan, Prog. Photovoltaics-Res. Appl. **23**, 437 (2015).
[27] J. M. Burst *et al.*, Nat. Energy **1**, 16015 (2016).
[28] A. Kanevce, M. O. Reese, T. M. Barnes, S. A. Jensen, and W. K. Metzger, J. Appl. Phys. **121**, 214506 (2017).
[29] J.-H. Yang, W.-J. Yin, J.-S. Park, W. Metzger, and S.-H. Wei, J. Appl. Phys. **119**, 045104 (2016).
[30] D. Krasikov and I. Sankin, J. Mater. Chem. A **5**, 3503 (2017).
[31] K. Biswas and M.-H. Du, New J. Phys. **14**, 063020 (2012).
[32] E. Menéndez-Proupin and W. Orellana, J. Phys. Conf. Ser. **720**, 012031 (2016).
[33] H. Peng, D. O. Scanlon, V. Stevanovic, J. Vidal, G. W. Watson, and S. Lany, Phys. Rev. B **88**, 115201 (2013).
[34] G. Kresse and D. Joubert, Phys. Rev. B **59**, 1758 (1999).
[35] J. Paier, R. Hirschl, M. Marsman, and G. Kresse, J. Chem. Phys. **122**, 234102 (2005).
[36] S. Steiner, S. Khmelevskyi, M. Marsmann, and G. Kresse, Phys. Rev. B **93**, 224425 (2016).
[37] G. I. Csonka, J. P. Perdew, A. Ruzsinszky, P. H. T. Philipsen, S. Lebègue, J. Paier, O. A. Vydrov, and J. G. Ángyán, Phys. Rev. B **79**, 155107 (2009).
[38] A. V. Krukau, O. A. Vydrov, A. F. Izmaylov, and G. E. Scuseria, J. Chem. Phys. **125**, 224106 (2006).
[39] C.-H. Su, J. Appl. Phys. **103**, 084903 (2008).
[40] D. Strauch, CdTe: lattice parameters, in *New Data and Updates for several III-V (including mixed crystals) and II-VI Compounds*, Landolt-Börnstein - Group III Condensed Matter, Vol. 44E, edited by U. Rössler (Springer-Verlag, Berlin, Heidelberg, 2012).
[41] J. A. Chan, S. Lany, and A. Zunger, Phys. Rev. Lett. **103**, 016404 (2009).
[42] H. Peng and S. Lany, Phys. Rev. B **85**, 201202(R) (2012).
[43] S. L. Dudarev, G. A. Botton, S. Y. Savrasov, C. J. Humphreys, and A. P. Sutton, Phys. Rev. B **57**, 1505 (1998).
[44] S. Lany and A. Zunger, Model. Simul. Mater. Sci. **17**, 084002 (2009).

[45] See Supplemental Material at http://link.aps.org/supplemental/10.1103/PhysRevB.98.054108 for (1) *U*/*V* parameters; (2) the FERE energies and enthalpies of formation for 23 compounds; (3) the projected electronic density of states of Cd interstitial neighbored by four Te; (4) the projected electronic density of states of Cd interstitial neighbored by four Cd; (5) the transition level $(0/2+)$ of a Te vacancy.
[46] S. Lany and A. Zunger, Phys. Rev. B **81**, 113201 (2010).
[47] V. Stevanovic, S. Lany, X. Zhang, and A. Zunger, Phys. Rev. B **85**, 115104 (2012).
[48] D. D. Wagman, W. H. Evans, V. B. Parker, R. H. Schumm, I. Halow, S. M. Bailey, K. L. Churney, and R. L. Nuttall, J. Phys. Chem. Ref. Data **11**(Suppl. 2) (1982).
[49] K. Yamaguchi, K. Hongo, K. Hack, I. Hurtado, and D. Neuschütz, Mater. Trans. **41**, 790 (2000).
[50] M. Tuteja, P. Koirala, V. Palekis, S. MacLaren, C. S. Ferekides, R. W. Collins, and A. A. Rockett, J. Phys. Chem. C **120**, 7020 (2016).
[51] M. Tuteja, A. B. Mei, V. Palekis, A. Hall, S. MacLaren, C. S. Ferekides, and A. A. Rockett, J. Phys. Chem. Lett. **7**, 4962 (2016).
[52] D. M. Waters, D. Niles, T. A. Gessert, D. Albin, D. H. Rose, and P. Sheldon, in *2nd World Conference and Exhibition of Photovoltaic Solar Energy Conversion* (Web, Vienna, Austria, 1998).
[53] J.-H. Yang, J.-S. Park, J. Kang, W. Metzger, T. Barnes, and S.-H. Wei, Phys. Rev. B **90**, 245202 (2014).
[54] J. H. Yang, L. Shi, L. W. Wang, and S. H. Wei, Sci. Rep. **6**, 21712 (2016).
[55] D. M. Hofmann, P. Omling, H. G. Grimmeiss, B. K. Meyer, K. W. Benz, and D. Sinerius, Phys. Rev. B **45**, 6247 (1992).
[56] A. Alkauskas, P. Broqvist, and A. Pasquarello, Phys. Rev. Lett. **101**, 046405 (2008).
[57] W. Martienssen and H. Warlimont, *Handbook of Condensed Matter and Materials Data* (Springer, Berlin, 2005).
[58] S. Lany and A. Zunger, Phys. Rev. B **78**, 235104 (2008).
[59] J. Pan, Y.-T. Cheng, and Y. Qi, Phys. Rev. B **91**, 134116 (2015).
[60] S. B. Zhang and J. E. Northrup, Phys. Rev. Lett. **67**, 2339 (1991).
[61] K. Biswas and S. Lany, Phys. Rev. B **80**, 115206 (2009).
[62] F. T. J. Smith, Metall. Mater. Trans. B **1**, 617 (1970).